Compact High-Turn-Ratio Transformer Design for Remotely Operated Underwater Vehicles

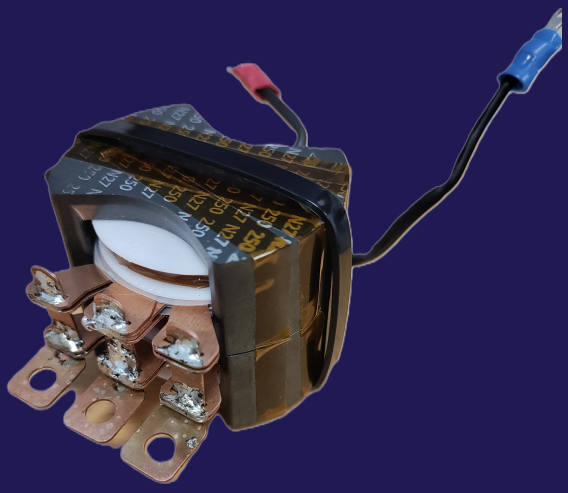

Jeppe Vilsøe Jensen

Power Electronics and Drives, PED4, 2025-1

Master Thesis

AALBORG UNIVERSITY
STUDENT REPORT

AAU Energy
Aalborg University
9220 Aalborg Øst
Pontoppidanstræde 111
http://www.energy.aau.dk/

Title:
Compact High-Turn-Ratio Transformer Design for Remotely Operated Underwater Vehicles

Theme:
Master Thesis

Project Period:
Spring Semester 2025

Project Group:
PED4-1051

Participant(s):
Jeppe Vilsøe Jensen

Supervisor(s):
Hongbo Zaho
Ariya Sangwongwanich
Gao Liu
Jannick Kjær Jørgensen

Page Numbers: 34

Date of Completion:
May 27, 2025

Abstract:

This thesis presents the development and evaluation of a compact, high-turn-ratio transformer intended for use in a power converter within a remotely operated underwater vehicle (ROV). The existing system, developed by AAL Power Group, utilizes a transformer manufactured by PREMO, which is constrained by an inadequate turn ratio of 30:1. This limitation restricts the input voltage from a 1000 V to 750 V, thereby reducing the system's ability to efficiently deliver 2 kW of power through a 300-meter cable.

To address this issue, a custom transformer with a 40:1 center-tapped winding configuration was developed. The new transformer design employs a semi-planar structure, which easily allows for a high number of turns one side and high current on the other. The design objectives was to minimizing secondary-side leakage inductance and increasing primary-side leakage inductance, to improve the performance of the phase-shifted full-bridge (PSFB) converter topology compared to the PREMO transformer.

To meet these objectives, a combination of 3D CAD modeling (SolidWorks) and finite element method (FEM) simulations (COMSOL) was used to guide the design process. However, notable discrepancies between simulated and experimental results were observed, primarily due to modeling simplifications and uncertainties in material properties.

Despite these challenges, the final prototype achieved a 35% reduction in secondary-side leakage inductance and doubled the primary-side leakage inductance compared to the original PREMO transformer. While key design values were successfully validated through laboratory testing, integration into the full converter system remains as future work.

Resume

Dette speciale omhandler udviklingen af en kompakt høj-vindingsforhold transformer til brug i en strømforsyning i en fjernstyret undervandsdrone (ROV). Projektet blev igangsat på baggrund af Aalborg Power Group (APG), som havde identificeret et problem med den eksisterende transformer, leveret af producenten PREMO. Den oprindelige transformer havde en vindingsforhold på 30:1, hvilket betød, at det maksimale inputspændingsniveau måtte begrænses til 750 V i stedet for det ønskede 1000 V. Dette ødede tabet igennem det 300m lange kabel forbundet til ROV'en. Målet med projektet var derfor at udvikle en ny transformer med et forbedret vindingsforhold på 40:1 og reducer sekundær lækageinduktans, øge den primære læk induktans, og samtidig sikre at den kunne passe ind i de fysiske begrænsninger af ROV'ens kompakte design.

Designet af transformeren blev udført i tre faser: teoretisk design, digitalt design og fysisk konstruktion. Den teoretiske fase omfattede beregninger til at finde en kerne og give et estimat af tab. I den digitale fase blev transformerens geometri modelleret i SolidWorks, og magnetiske egenskaber blev simuleret med Finite Element Method (FEM) i COMSOL. Designet anvendte en semi-planar struktur med en splittet sekundær vikling i kobberplader og en primær vikling bestående af Litz-tråd. Formålet med denne struktur var at opnå høj magnetisk kobling og samtidig styre lækageinduktansen.

Der blev foretaget laboratorie eksperimenter, herunder impedansmålinger, lækstrømstest ved op til 1400 V samt verifikation af vindingsforhold. Resultaterne viste, at den nye transformer opnåede et omsætningsforhold på 39,89:1, hvilket er meget tæt på det ønskede mål. Den sekundære lækageinduktans blev reduceret med cirka 35% sammenlignet med PREMO-transformeren, og den primære lækageinduktans blev næsten fordoblet, hvilket er fordelagtigt for strømforsyningen.

På trods af uoverensstemmelser mellem simulerede og målte værdier, primært for PREMO transformeren var grunden usikkerheden om kernematerialets egenskaber og genneralt simplificeret geometri, bidrog simulationsværktøjerne til forståelsen af designet. Det konkluderes, at et semi-planar struktur er en effektiv løsning for kompakte, højt ydende transformere i krævende applikationer så som undervandsdroner.

Fremtidigt arbejde bør fokusere på termisk simulering, yderligere forbedring af isolationsstyrke, integration af transformeren i den faktiske konverter, eventuel undersøge muligheden for at anvende fuldt planer design, hvilket kan forbedre simuleringens nøjagtighed og forsimple produktionen. Projektet har demonstreret potentialet ved digitalt drevet transformatorudvikling og lagt fundamentet for videre optimering og implementering i praksis.

Preface

The following software and hardware have been used during the writing of this report:

- Overleaf for text processing.
- Solidworks for design.
- Comsol for modelling and simulation.
- Inkscape for figure composing.
- Draw.io for figure composing.
- Microsoft 365 for data processing and sharing.
- ChatGPT for Spelling and Grammar.
- Le Chat for Spelling and Grammar.

Aalborg University, May 27, 2025

Jeppe Vilsøe Jensen
jvje19@student.aau.dk

Nomenclature

Units of measurement		
Symbol	**Explanation**	**Unit**
A_L	Inductance constant of the core	nH/turn^2
$B_{\max}$	Maximum flux density	T
C_{wpri}	Primary winding capacitance	pF
C_{wsec}	Secondary winding capacitance	nF
C_{wss}	Secondary-to-secondary capacitance	nF
$C_{\text{ww1}}, C_{\text{ww2}}$	Interwinding capacitance	pF
f	Switching frequency	Hz
$I_{\max}$	Maximum primary current	A
k	Couplings coefficient	
L_{pri}	Primary winding inductance	H
L_{sec}	Secondary winding inductance	H
$L_{\text{pri,leak}}$	Primary leakage inductance	H
$L_{\text{pri,mag}}$	Primary magnetisation inductance	H
$L_{\text{sec,leak}}$	Secondary leakage inductance	H
$L_{\text{sec,mag}}$	Secondary magnetisation inductance	H
L	Length	m
N_{pri}	Number of turns on primary winding	turns
N_{sec}	Number of turns on secondary winding	turns
n	Turn ratio	–
P	Power	W
R_{pri}	DC resistance of primary winding	Ω
R_{sec}	DC resistance of secondary winding	mΩ
V_{in}	Input voltage	V
V_{out}	Output voltage	V
δ	Skin depth	mm
μ_0	Permeability of free space	H/m
μ_r	Relative permeability	–
ϕ	Diameter	m
ρ	Resistivity of conductor material	Ω·m

Contents

1 Introduction

With the growing number of sustainable energy solutions, particularly in offshore production, there is an increasing need for cost-effective solutions to maintain and construct these sites [1]. Therefore, Aalborg Power Group (APG)[2] has been commissioned to develop a new power system for an underwater remotely operated vehicle (ROV). An ROV is an underwater drone, as seen in Figure 1.1, connected to the surface through a cable over 300 meters long to maintain communication.

The new power system is designed to replace the existing battery design, which currently provides only half an hour of operation time. To increase the operation time, the battery pack will be replaced with direct power from the surface. The ROV requires 2 kW at 20 V. However, transferring this power through a 300-meter cable would result in significant losses. To mitigate these losses, the voltage in the cable will be increased to 1000 V. To facilitate this change, APG needs to develop a high step-down converter.

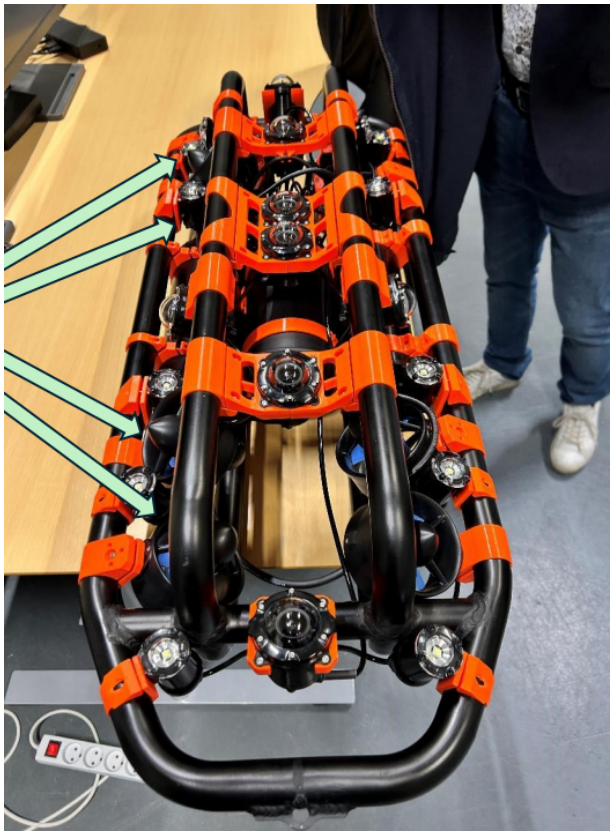

Figure 1.1 The Remote Operated Vehicle.

During the development, they encountered a problem that has prevented them from fulfilling the intended requirements for the system. In general, the problem has been narrowed down to the transformer, which has too low of a turn ratio, meaning that the input voltage have to be reduced to $750V$. The goal of this project is to develop a new transformer to fix the issue.

1.1 The Power System

The power system, as seen in Figure 1.2, is designed to deliver 2 kW of power to an ROV through a 300 meter long cable at $20V$. To deliver $2kW$ of power to the ROV through this 300-meter-long cable, to do this efficiently the voltage is boosted to $1000V$ on the boat. This is done using a commercially available power supply. However, this solution cannot be implemented on the ROV due to the limited available space and custom size requirements.

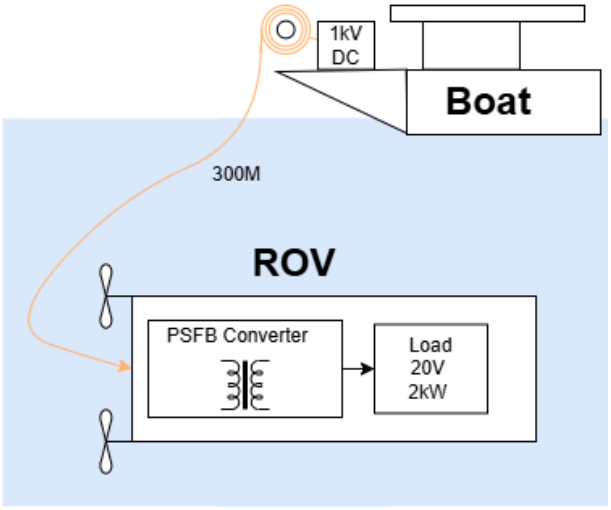

Figure 1.2 Overview of the Power system. The transformer in the PSFB converter is the problem.

To reduce the voltage from 1000V down to 20V, APG decided to use a phase-shifted full-bridge topology (PSFB). The advantages of this topology are that it can step down a high amount of power using a transformer. It can do this efficiently with the use of a transformer, and it also allows for soft-switching operation, further increasing efficiency.

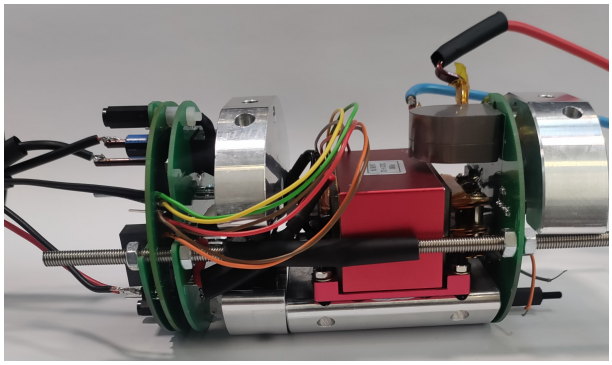

Figure 1.3 APG PSFB Converter for the ROV.

Figure 1.4 The PREMO Transformer [3] used in the converters.

In developing the converter, it was found that the converter could not fulfill the requirements of the system. For the system to deliver 20V, the voltage of the cable had to be reduced to 750V. This was caused by the too low turn ratio of only 30:1 in the transformer. For optimal performance of the converter, the turn ratio needs to be increased to at least 40:1. However, due to the high turn ratio of the transformer and the specific requirements, no such transformers are easily available and therefore need to be custom developed.

1.2 Problem Formulation

A transformer is an essential part of modern power electronics and brings many advantages. However, finding the right transformer can be impossible due to many specific use cases. Therefore, designing a custom transformer for the use case is important to fulfill the requirements. From this, the following problem statement is formulated.

How to design and optimize a high turn ratio transformer for a Phase Shifted Full Bridge Converter using digital tools?

1.2.1 Hypothesis

- It is possible to analyse and optimize high turn ratio transformer Efficiency, Volume and inductive elements using Finite element method.
- It is possible to have a Large Primary Leakage inductance and a Small secondary leakage inductance using semi-planar transformer.
- It is possible to accurate Simulate a Transformer using Finite element method..

1.2.2 Objectives

In this project the main objectives are:

- Analyse and modelling the PREMO Transformer for the Transformer equivalent circuit and understand the physical properties.
- Review fundamental structures of PREMO manufactured high-turn-ratio transformer.
- Designing a high-turn-ratio transformer and analyse it using Finite element method.
- Optimize the design based on the application requirement.
- Develop and test the prototype transformer to get the Transformer equivalent circuit.
- Implement it into the converter.
- Understand the working Phase shifted full-bridge converter.

1.2.3 Design Requirements

The transformer must meet the following design specifications:

- **Topology:** Centre-tapped transformer design.
- **Turn Ratio:** 40:1, with a split secondary winding configuration (40:1+1).
- **Power Rating:** Capable of handling up to 2 kW.
- **Physical Dimensions:** The transformer must fit within a cylindrical volume with an inner diameter of 80 mm and a maximum length of 70 mm, with an ideal target length of 50 mm to minimize volume.
- **Leakage Inductance:**
  - **Primary Side:** Increase the on leakage inductance. compared to the PREMO transformer.
  - **Secondary Side:** Must be less than 130 nH, which is lower than the reference PREMO transformer.
- **Resonant Frequency:** Must exceed 1 MHz to avoid interference with system operation.

1.2.4 Limitations

The project has the following limitations:

- The impact of different materials on the performance of the transformer is not investigated. All components used in the construction are off-the-shelf and not specifically optimized for electrical or thermal performance.
- Capacitance effects are not included in the transformer simulations. This is primarily due to time constraints and the increased complexity associated with accurately modeling inter-winding and parasitic capacitances, particularly in traditional winding structures.

2 State of the Art

2.1 The Phase Shifted Full Bridge Converter

The Phase Shifted Full Bridge (PSFB) converter is a topology that enables highly efficient power conversion using a transformer and soft switching. This topology is more power efficient compared to a forward or flyback converter, and it serves as a stepping stone toward more advanced converter types such as LLC resonant converters or the Dual Active Bridge, which features a full-bridge converter on each side of a transformer. The schematic of the topology can be seen in Figure 2.1. Starting from the left, the switches can be seen in a full-bridge configuration. Power is transferred through a transformer, then rectified, and finally passed through a filter to smooth the output.

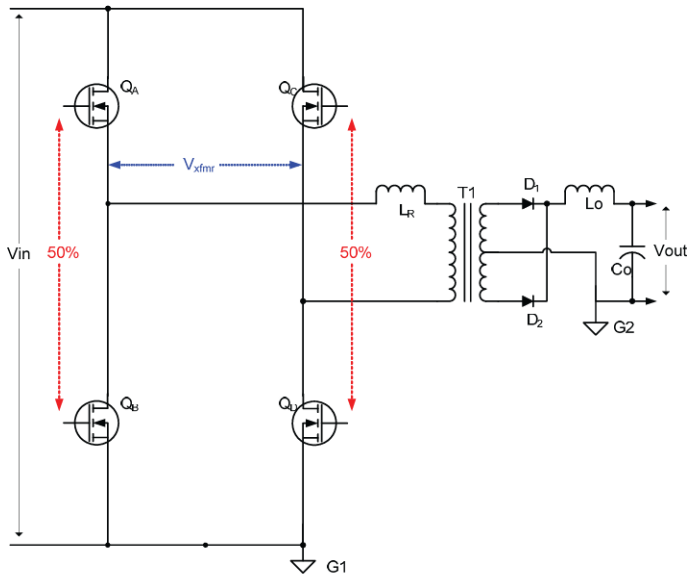

Figure 2.1 Schematic of a PSFB with a centre-tapped transformer. [4]

What distinguishes the Phase Shifted Full Bridge from a standard full-bridge converter is the method of switch control, as illustrated in Figure 2.2. In this scheme, switches are operated diagonally for example, switches Q_A and Q_D turn on simultaneously, while Q_B and Q_C remain off. The timing between Q_D and Q_C is shifted by a certain amount, creating an overlap. The greater the overlap that is, as the operation approaches that of a conventional full-bridge the higher the resulting output voltage.

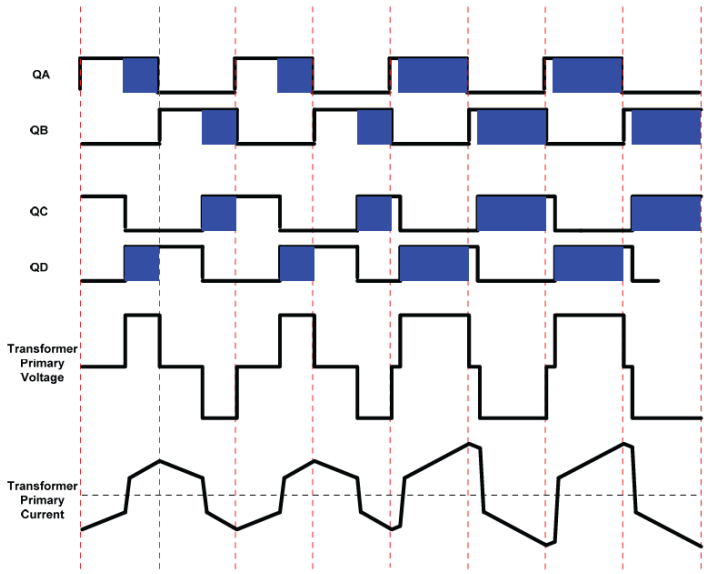

Figure 2.2 Waveforms and turn cycles of a .[4]

With the switches being out of phase, the output voltage can be adjusted. This phase shift enables soft switching, meaning that neither the full current nor the full voltage is experienced during the switching transitions. An example of this in the PSFB converter occurs during the transition from the state where Q_A and Q_D are on to the state where Q_B and Q_C are on. This is achieved by first turning off Q_D, then turning on Q_C, which allows the current to continue flowing. With Q_C now on, Q_A can be turned off, and finally Q_B is turned on. In this way, soft switching is achieved. This greatly increases efficiency during operation and reduces stress on the components.

2.1.1 Transformers Types

In the Phase Shift Full Bridge (PSFB) converter, two different types of transformers can be used, each with its own advantages and disadvantages: the traditional transformer and the center-tap transformer. The center-tap configuration is used in the APG converter, as shown in Figure 2.1. However, it is still important to discuss the differences between the two transformer types.

At first glance, the traditional transformer used with a full-bridge rectifier requires more diodes compared to the center-tap configuration. This means that, for the same number of turns, the traditional transformer setup involves more components than the center-tap transformer.

When analyzing waveform interactions with the transformer, both configurations behave similarly on the primary side, where alternating current is present. However, on the secondary side of a traditional transformer, the magnetic field alternates in both positive and negative directions, leading to greater core losses. In contrast, the center-tap transformer conducts through only one winding during each half-cycle — the upper winding during positive cycles and the lower winding during negative half-cycles — resulting in reduced core losses. However, this configuration increases the load stress on the diodes compared to the traditional transformer.

2.2 Fundamentals of Transformer

Before beginning the design of the transformer, it is essential to understand the implications of various design choices. While transformers are typically characterized by the turns ratio between the primary and secondary windings, this is only part of the story. To fully grasp a transformer's impact on a converter, it is necessary to examine its equivalent circuit in detail, as illustrated in Figure 2.3.

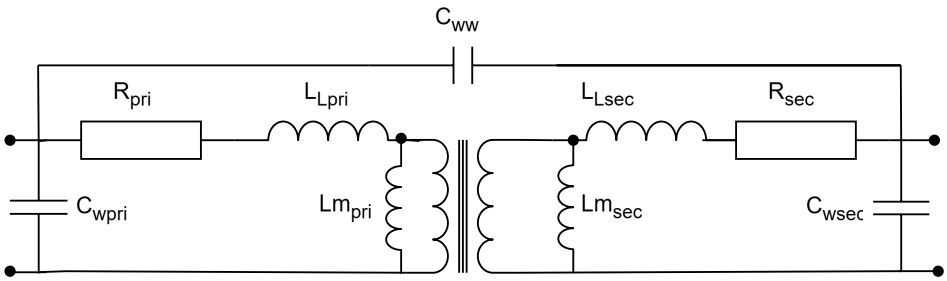

Figure 2.3 Transformer Equivalent Circuit. [5]

There are generally two key equations used during the initial design of a transformer. Other transformer equations are often applied retrospectively, as many parameters depend heavily on the specific manufacturing process.

The first key equation in transformer design is the turns ratio, which is typically defined by the number of turns in the primary and secondary windings. However, a more comprehensive representation also considers the inductance and voltage relationships.The ideal turns ratio is given by Equation 2.1:

$$n = \frac{N_{pri}}{N_{sec}} = \frac{V_{pri}}{V_{sec}} = \sqrt{\frac{L_{pri}}{L_{sec}}} \tag{2.1}$$

Where N_{pri} and N_{sec} are the number of turns in the primary and secondary windings, respectively. V_{pri} and V_{sec} are the voltages across each winding. Finally, L_{pri} and L_{sec} are the self-inductances of the primary and secondary windings. These inductances can be estimated using the following formula:

$$L = A_L \cdot N^2 \tag{2.2}$$

Here, A_L is the inductance factor (typically given in nH or µH per turn squared), and N is the number of turns.

In practice, the presence of **leakage inductance** causes deviation from the ideal voltage transfer. As a result, the actual voltage on the secondary side is reduced. The relationship accounting for imperfect magnetic coupling is:

$$V_{sec} = k \cdot \frac{N_{sec}}{N_{pri}} \cdot V_{pri} \tag{2.3}$$

where k is the *coupling coefficient* of the transformer, with $0 < k \leq 1$. A coupling coefficient of $k = 1$ indicates perfect magnetic coupling with no leakage inductance.

The second key equation is used to calculate the peak flux density, which is critical for determining whether the magnetic core is approaching saturation. This is shown in Equation 2.4:

$$B_{max} = \frac{\mu_r \cdot \mu_0 \cdot N \cdot I_m}{A_l} \tag{2.4}$$

The peak flux density depends on the core permeability, the number of winding turns, and the peak current through the winding. This relationship assumes separate primary and secondary windings. However, if the windings are interleaved, the effective number of turns must be adjusted to account for increased flux linkage and mutual coupling. In interleaved configurations, the magnetic flux is more evenly distributed, resulting in reduced peak flux density. For instance, if both the primary and secondary windings are symmetrically split into two sections and interleaved, the maximum flux density can be approximately halved.

These two equations are typically used for the initial design phase. The following equations support winding design and loss estimation.

The first of these is used to estimate the skin depth, which is crucial when handling high-frequency AC currents. The depth at which current effectively flows is determined by the frequency. The skin depth is calculated using:

$$\delta = \sqrt{\frac{2 \cdot \rho}{2 \cdot \pi \cdot f \cdot \mu_r \cdot \mu_0}} \tag{2.5}$$

For copper at a switching frequency of 100 kHz, the skin depth is approximately 0.2 mm. Once the skin depth is known, it can be used to determine the maximum effective thickness of the winding conductor. Additional equations are then used to scale the winding dimensions and estimate losses to ensure acceptable thermal and electrical performance.

2.2.1 Winding Types

The windings in transformers can generally be categorized into two types, both of which are discussed in this project: wire windings and planar windings.

Wire Winding

Wire winding has traditionally been used in transformers. At low frequencies, solid wire is typically employed. At higher frequencies, Litz wire—composed of multiple insulated strands twisted together—is used to mitigate the skin effect. However, Litz wire can introduce proximity effects [6], where current flowing in one strand induces eddy currents in adjacent strands, distorting the current distribution.

Wire winding is the most cost-effective method for transformer construction. Despite its affordability, it offers several advantages, including the ability to achieve a high number of turns, a compact form factor, and a well-established manufacturing process compared to planar windings.

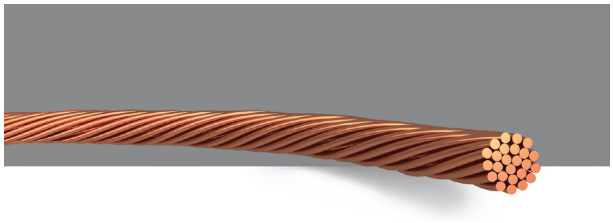

Figure 2.4 Litz Wire winding[7]

Planar

Planar windings consist of copper traces etched on a PCB or cut from copper plates. This method produces highly uniform windings that can be easily layered and interleaved, resulting in compact and thermally efficient designs. However, achieving high turn ratios may be challenging, especially without multiple PCB layers. Cut-out planar windings are well-suited for applications requiring high current capacity

Figure 2.5 Planar windings

Semi-Planar

Semi-planar windings, such as those used in PREMO transformers, provide a hybrid solution that combines features of both wire and planar technologies. This approach offers high turn counts on one side and high current capability on the other, striking a balance between flexibility, efficiency, and thermal management.

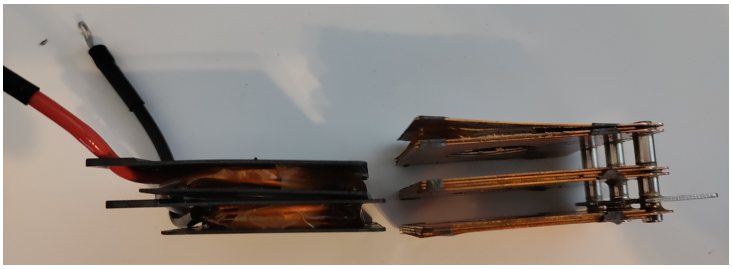

Figure 2.6 PREMO Semi-Planar windings split up into two with wire winding on the left and planar on the right.

2.3 Evaluvation of PREMO Transformer

To gain an understanding of the transformer that APG is using in the converter, note that the transformer is sourced from the company PREMO[3] and will henceforth be referred to as such. The transformer can be seen in the following figure.

Figure 2.7 PREMO transformer used in the APG Converter. [3]

2.3.1 Testing

The testing techniques discussed in the following sections apply primarily to traditional transformers [5]. Only minor modifications are required to test a center-tapped transformer, where the same measurements are simply repeated on the second winding. The equivalent circuit for a center-tapped transformer is shown in Figure 2.8.

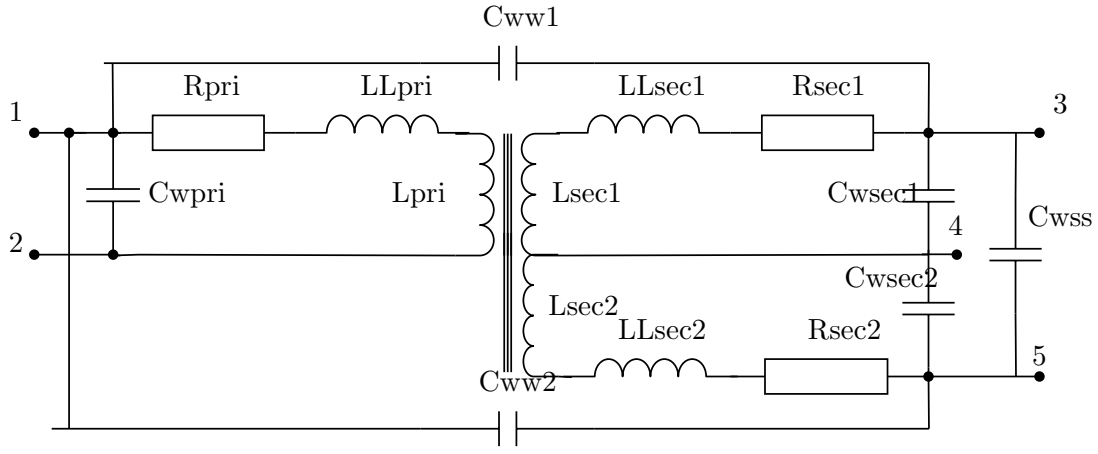

Figure 2.8 Equivalent circuit for center-tapped transformer.

Magnetization Inductance

Magnetization inductance is the inductance commonly associated with energy transfer in a transformer. It defines the turn ratio and governs how energy is magnetically transferred between the windings. It is measured using an open-circuit test, where the opposite side of the transformer is left unconnected.

Leakage Inductance

Leakage inductance, also known as stray inductance, refers to the portion of the magnetic field that does not contribute to the coupling between windings. In Figure 2.8, it is represented in series with the primary inductor. While leakage inductance is typically minimized in most applications to avoid its detrimental effects, it can be intentionally utilized in certain designs—such as the one discussed here. To measure leakage inductance, the secondary winding is short-circuited, and the inductance is measured from the primary side.

Winding Resistance

The DC resistance of the transformer windings corresponds to the resistance of the copper wire and can be measured directly with an ohmmeter across each winding. However, the effective resistance during operation is frequency-dependent due to phenomena such as the skin effect, which reduces the effective conductive cross-sectional area and thereby increases the AC resistance. Additionally, the proximity effect also influences current distribution in the conductors, further impacting the effective resistance at higher frequencies.

Coupling Capacitance

The coupling capacitance between the primary and secondary windings can be measured by short-circuiting both windings and measuring the capacitance between them using an LCR meter[5]. This coupling is what transfers EMI noise from one side to the other.

Winding Capacitance

Winding capacitance is determined by finding the self-resonant frequency of one side of the transformer while leaving the opposite side open. With the known inductance value, the capacitance can then be calculated using the resonant frequency formula. This resonant frequency can be used to enable soft switching in the converter.

2.3.2 The Lab Setup and Results

The laboratory setup for testing the TEC of the PREMO transformer utilizes a Keysight E4990A impedance analyzer[8] with a 16047E test fixture[9] for connection. The impedance analyzer uses the same measurement points as manual methods, but the values are derived from an impedance curve using curve fitting. This entire process is handled internally by the analyzer.

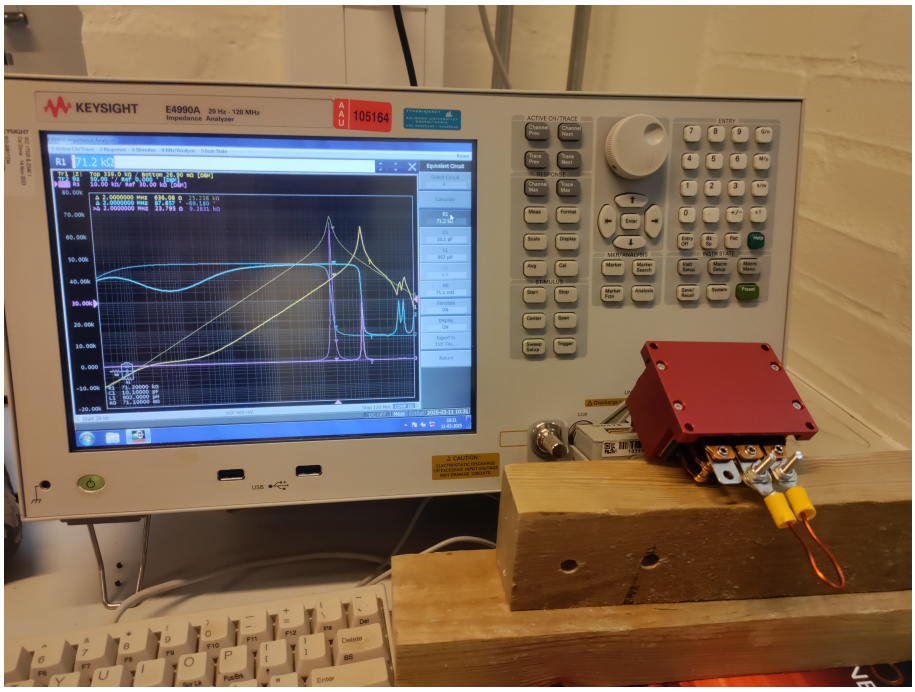

Figure 2.9 Laboratory setup using the Keysight impedance analyzer on the PREMO transformer[8][9]

The results from the tests are presented in the following table, which includes values corresponding to the TEC. The table lists inductances, resistances, and capacitances based on the specified measurement configuration.

Measurement	Value	Unit	Measurement Points	Connected Together	Open
L_{mpri}	902	μH	1.2		all
L_{msec1}	1.13	μH	3.4		all
L_{msec2}	1.13	μH	4.5		all
Total Leakage Inductance					
L_{lpri}	8.2	μH	1.2	3.4, 5	
L_{lsec1}	137	nH	3.4	1.2	4
L_{lsec2}	131	nH	4.5	1.2	3
DC Winding Resistance					
R_{pri}	2.6	Ω	1.2		all
R_{sec1}	3.2	mΩ	3.4		all
R_{sec2}	3.0	mΩ	4.5		all
Coupling Capacitance					
C_{ww1}	62.3	pF	1.3	1.2 & 3.4	5
C_{ww2}	62.5	pF	1.5	1.2 & 4.5	3
Winding Capacitance					
C_{wpri}	10.1	pF	1.2		all
C_{wsec1}	9.72	nF	3.4	4.5	3.4
C_{wsec2}	9.59	nF	4.5	3.4	4.5
C_{wss}	2.59	nF	3.5		all

Table 2.1 Test results and setup configuration for the PREMO transformer equivalent circuit

2.3.3 Structure of the PREMO Transformer

To gain a deeper understanding of the PREMO transformer [3] and its operation, the transformer was disassembled and analyzed. Figure 2.7 shown at the beginning of this section.

The first step in the disassembly process was to remove the red protective cover to access the core. Since the core is held together with epoxy, it had to be broken to separate the parts. The result is shown in Figure 2.10.

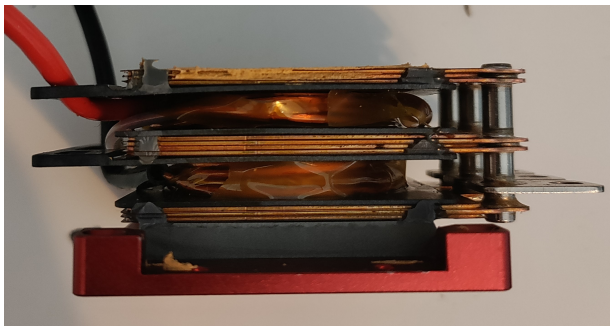

Figure 2.10 PREMO transformer with the top and side of the core removed, providing direct access to the windings.

From Figure 2.10, the interleaved winding arrangement is visible. The secondary winding consists of three layers, with the top and bottom layers each containing 3 plates, while the middle layer contains 4 plates. This configuration ensures that each side of the center-tapped winding has 5 turns, all connected in parallel.

The primary winding is made of Litz wire and is divided into two sections, each with 15 turns, interleaved between the planar windings of the secondary side. The primary winding is wound around a plastic bobbin to facilitate manufacturing, with the plates being identical but flipped depending on their orientation. The core is believed to be ungapped, although this is difficult to confirm due to the nature of the disassembly. This design aims to reduce primary leakage inductance by interleaving the primary windings with the secondary windings.

2.3.4 FEM analysis of a PREMO Transformer

To evaluate the simulation tools and gain experience using COMSOL [10], the PREMO transformer was modeled in CAD and imported into COMSOL. Since the transformer was disassembled beforehand, it was relatively straightforward to recreate the design in SolidWorks and transfer the model into COMSOL.

Figure 2.11 presents an exploded view. The most challenging part of the CAD design was modeling the primary winding, as the real-world windings are closely packed. In this design, the windings are spaced further apart, which is likely to cause the largest deviation from the actual physical design.

In COMSOL, the simulation focuses only on the inductive values—magnetization and leakage inductance—since the capacitance between windings is difficult to model accurately in CAD. Another limitation is the lack of information about the core material, which significantly

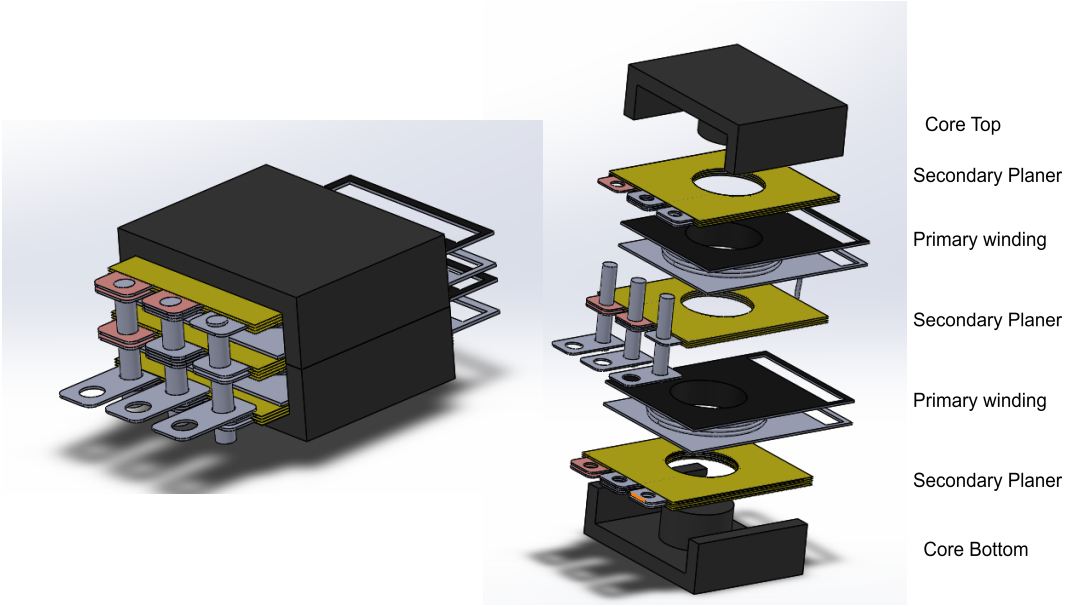

Figure 2.11 PREMO Transformer recreated in SolidWorks[11] and an exploded view for increased understanding.

affects simulation accuracy. Therefore, the objective is to produce results that are qualitatively comparable to real-world measurements.

The COMSOL simulation setup is documented in Appendix A.

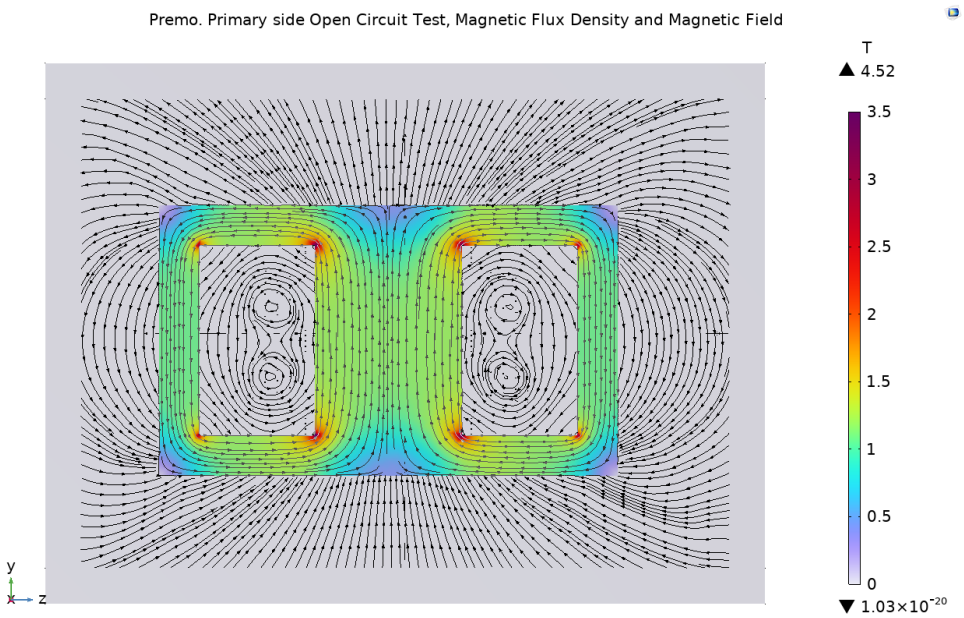

Figure 2.12 Primary Side Open-Circuit Simulation: Magnetic Flux Density and Magnetic Field, PREMO transformer in Comsol[10]

Figure 2.12 shows the magnetic field simulation results, with the transformer cut in half for clarity. The two primary windings are easily visible due to the magnetic field lines forming small circular patterns. The peak flux density is notably high—exceeding $1T$—which is likely due to the incorrect core material used in the simulation. Additionally, the sharp corners in the model cause an increase in localized peak flux density; filleting the corners would help reduce

this effect.

2.3.5 Comparison Between Simulations and Experimental

To better understand the differences between simulation and lab measurements, the inductive values are summarized in Table 2.2 for easy comparison.

Parameter	**PREMO Exp**	**PREMO Sim**	**PREMO Datasheet[3]**
$L_{\text{pri, mag}}$	0.9 mH	1.58 mH	0.915 mH ±25%
$L_{\text{pri, leak}}$	8.2 µH	16.2 uH	Max. 10µH
$L_{\text{sec, mag}}$	1.31 µH	1.76 µH	N/A
$L_{\text{sec, leak}}$	135 nH	N/A	N/A

Table 2.2 Comparison of inductance values from experimental measurements, simulation and datasheets

From Table 2.2, it can be observed that the simulation results deviate significantly from the experimental measurements, with simulated values ranging from 35% to 90% higher. While the datasheet values are generally correct, they lack precision. One of the main contributing factors to this discrepancy is the uncertainty regarding the actual core material, which has a substantial impact on inductance values in simulation. Additional deviations arise from modeling simplifications, such as exaggerated spacing between windings and the use of idealized sharp geometric edges. Ultimately, the accuracy of a simulation is directly dependent on the quality of its input data and the validity of its assumptions.

Furthermore, the secondary leakage inductance could not be accurately determined through simulation due to the simulation failed. As a result, no value could be extracted for this parameter. Further refinement of the simulation model and assumptions will be necessary to achieve more accurate and reliable outcomes.

3 Design

3.1 Design Process

The design of a transformer typically progresses through three main phases: Theoretical Design Phase, Digital Design Phase, and Physical Phase, where manufacturing and testing are performed. This workflow is illustrated in the design algorithm shown in Figure 3.1.

The first phase of the workflow is the Theoretical Design Phase, which involves the calculations to establish key electrical parameters such as turns ratio, flux density, and Power losses. The second phase, Digital Design Phase, introduces modern tools such as Computer Aided Design (CAD) and Finite Element Method (FEM) simulations, which are used to digitally model the transformer based on the theoretical parameters. These simulations allow for deeper insights into magnetic behaviour and help identify areas for optimization. The final phase is the physical realization of the transformer, followed by experimental validation and testing.

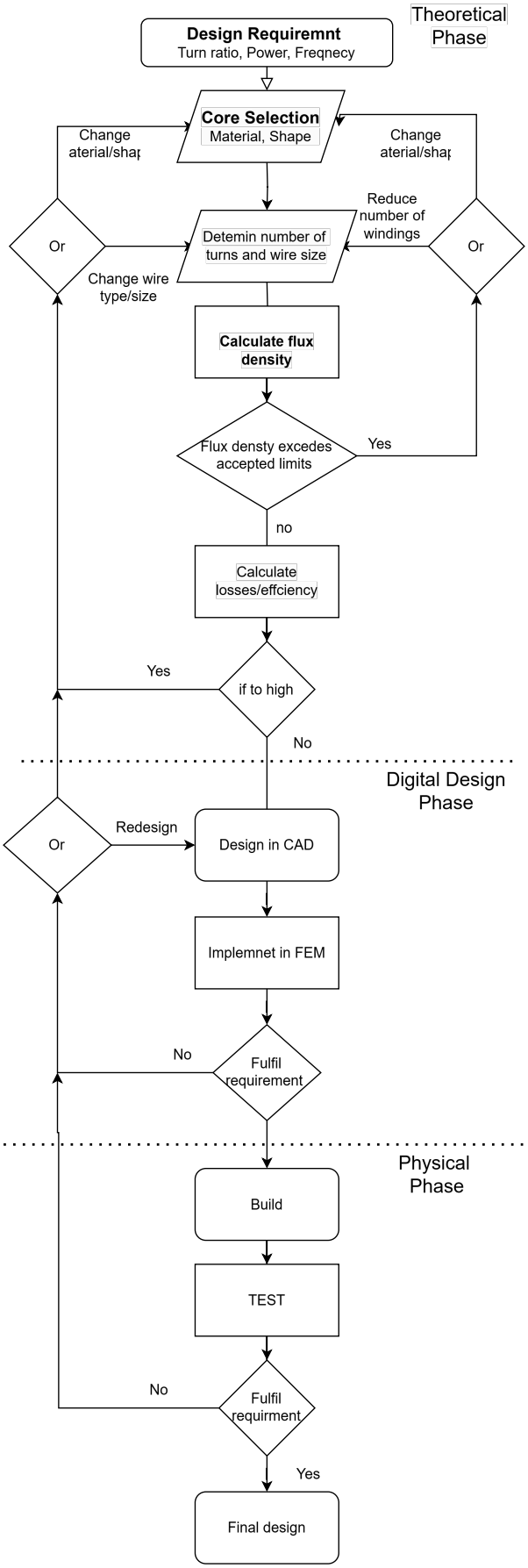

Figure 3.1 Flowchart for the design of a transformer.

3.2 Theoretical Design Phase

Before starting the transformer calculations, the key specifications of the converter must be defined. Based on the requirements from the APG system, the following design parameters were established:

- $V_{in} = 1000$ V
- $V_{out} = 20$ V
- $P = 2$ kW
- $f = 100$ kHz
- Turn ratio = 40 : 1 center tap
- $I_{\max} = 3.5$ A
- Size constraints: $\phi < 80$ mm, $L < 70$ mm

The first design choice involves selecting the transformer core. A variety of core types are available, including different E-cores, PM, PQ, and RM cores. For this project, the PM50/39 core from TDK [12] was selected. This core is available in both N87 and N27 materials and comes in gapped and ungapped versions.

Using Equation 2.4, the peak flux density was calculated. For the ungapped version, the peak flux density reached approximately 3.5 T, while the version with a 2.2 mm air gap reduced the peak flux to around 0.15 T. The saturation flux density for the chosen material is approximately 0.45 T, so the design must stay below 0.3 T to avoid approaching saturation. Due to this consideration, the gapped version of the core was selected for the final design.

To estimate core losses, the AI-powered tool Magnet [13, 14, 15], developed by Princeton University, was used. The tool predicted core losses of approximately 13 W, corresponding to a core efficiency of over 99%. These results were considered acceptable for the application.

3.3 Digital Design

With the core selected, the design of the new transformer adopts a semi-planar structure similar to the PREMO transformer. The secondary side consists of a single turn made from multiple parallel windings to ensure strong magnetic coupling. Unlike the PREMO design, this transformer inverts the interleaving arrangement: the primary side is split across three layers, while the secondary side is split across two. This structure is intended to minimize leakage inductance on the secondary side—where it is undesirable—and shift it to the primary side, where a controlled amount may be beneficial.

The primary windings are divided into three layers: 10 turns in the top and bottom layers, and 20 turns in the middle. The secondary side, which carries significantly higher current, consists of two planar windings—each with two parallel turns—spread across two layers, as illustrated in Figure 3.2.

3.3.1 Design Philosophy

Based on the APG system requirements, the transformer must achieve a turn ratio of $40:1+1$ and maintain minimal leakage inductance on the secondary side. Additionally, the resonant frequency of the transformer must be high enough to prevent interference with the rest of the converter system.

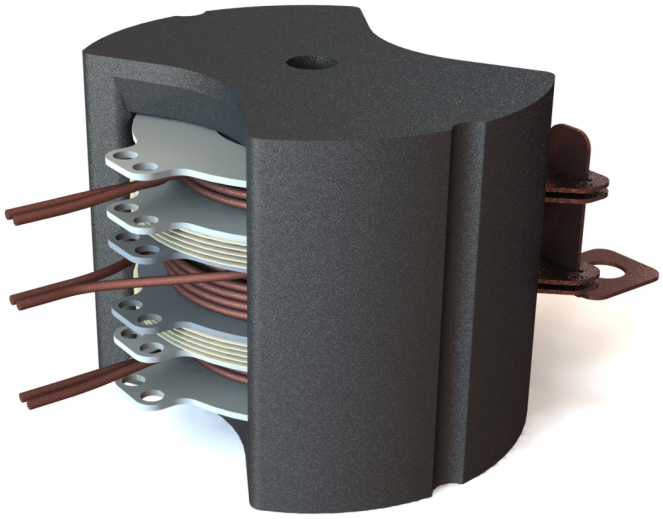

Figure 3.2 New semi-planar transformer design.

Primary Side

As shown in Figure 3.2, the primary winding is wound around a plastic bobbin for ease of assembly. The conductor used is Litz wire type CLI 200/120 [16], which consists of 120 strands of $\phi = 0.1$ mm wire, providing an equivalent cross-sectional area of 0.98 mm^2.

Secondary Side

The secondary side is designed to carry up to 100 A with only a single turn. To handle this current, planar windings made from 0.5 mm thick copper plates are used. The insulation between the plates is provided by 0.1 mm thick Mylar sheets.

Leakage Inductance

Leakage inductance represents the portion of magnetic flux that is not coupled between the primary and secondary windings [6]. It is primarily dictated by the physical layout of the windings. Minimizing leakage inductance requires improving the magnetic coupling between the windings, which can be achieved by tighter interleaving and shorter magnetic paths [17].

Winding Capacitance

Winding capacitance arises between adjacent turns or layers due to the voltage difference and the physical proximity of conductors. The capacitance is influenced by voltage, area, and separation

distance. Increasing the distance between windings reduces capacitance but can inadvertently increase leakage inductance. Therefore, a careful trade-off must be made during the design process to optimize both parameters.

Voltage Breakdown

To prevent internal short circuits, adequate voltage isolation must be ensured between and within the windings.

Secondary Side: The planar windings are insulated using Mylar film with a thickness of 0.1 mm, providing a dielectric strength exceeding 10 kV [18], which is more than sufficient for the operating voltages.

Primary Side: The primary windings use Litz wire type CLI 200/120, insulated with polyethylene (grade 1), which has an average thickness of 0.0115 mm [19]. The dielectric strength of polyethylene is approximately 18.9 kV/mm, translating to a breakdown voltage of roughly 283 V.

Given that the outer sections of the primary experience voltages up to 250 V and the center section up to 500 V, additional insulation is necessary. To increase isolation between winding layers, 65 μm Kapton tape is added, which has a breakdown strength of about 200 kV/mm [20]. This results in a breakdown voltage of approximately 13 kV between layers. With 4–5 turns per layer, the maximum inter-turn voltage is about 100–125 V, which remains well below the breakdown threshold.

3.3.2 Transformer CAD Design

The complete transformer design was created in SolidWorks. This software enables the modeling of individual components and full assemblies, as shown in Figure 3.3. A fully assembled CAD model facilitates easier integration into FEM simulation tools.

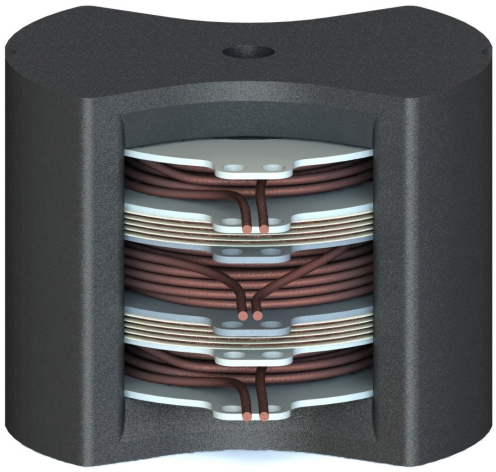

Figure 3.3 New transformer design from the primary side. Primary winding segments are not yet electrically connected but should be in series.

The primary winding is divided into three sections: two outer layers with 10 turns each and a middle layer with 20 turns. These are wound around a plastic bobbin, which includes mounting holes to secure the windings in place. The design encloses the secondary winding within the primary to help reduce secondary-side leakage inductance.

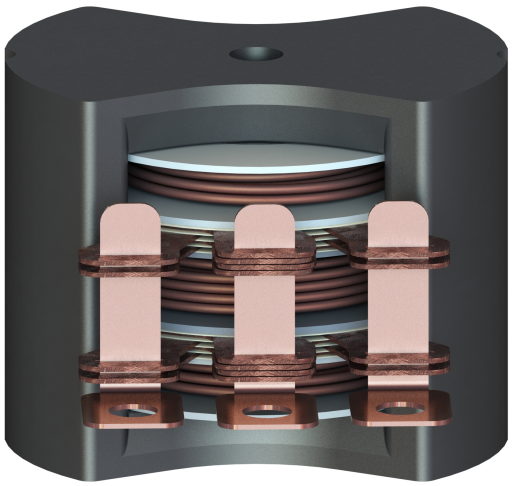

Figure 3.4 New transformer design: secondary side with terminal taps.

The secondary winding, as seen in Figure 3.4, is split into two layers. Each layer contains two windings in parallel, cut from a 0.5 mm copper plate. The connectors are also cut from the same material. The spacing between terminals matches that of the PREMO transformer to ensure compatibility. These taps carry the full load current and therefore experience the highest current density, but due to their short length, thermal concerns are minimal.

An exploded view of the full assembly is shown in Figure 3.5 to illustrate, how the components are stacked and integrated:

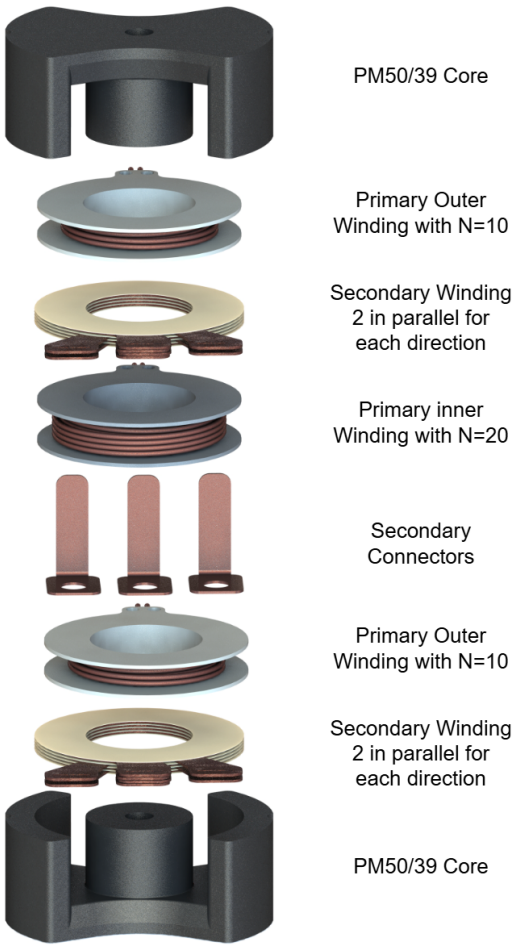

Figure 3.5 Exploded view of the new transformer design with component breakdown.

3.3.3 FEM Simulations

With the full CAD model completed, it was imported into COMSOL for simulation. The same tests conducted on the PREMO transformer were replicated to extract an equivalent circuit model. These include open-circuit and short-circuit simulations to evaluate inductive properties. As the core material is known in this case, more accurate and comparable results were expected. Simulation setup details are provided in Appendix A.

The simulated results are compared with theoretical calculations in Table 3.1:

	Calculated	Simulated
Lpri_Mag	0.4 mH	N/A
Lpri_Leak	N/A	N/A
Lsec_Mag	250 nH	298 nH
Lsec_Leak	N/A	194 nH

Table 3.1 Comparison of inductive results: calculated vs. simulated.

From the table, it can be seen that the simulated secondary magnetization inductance is slightly higher than the calculated value, which is within acceptable limits. The secondary leakage inductance is measured at 194 nH—about 50% higher than that of the PREMO transformer.

This is undesirable, as the goal was to minimize this value, but due to time constraints, the current design will be pursued.

As with previous simulations, the results for the primary inductance were inconclusive. However, by examining the field distribution in the cutaway view (Figure 3.6), valuable insight into the transformer's behaviour can still be obtained.

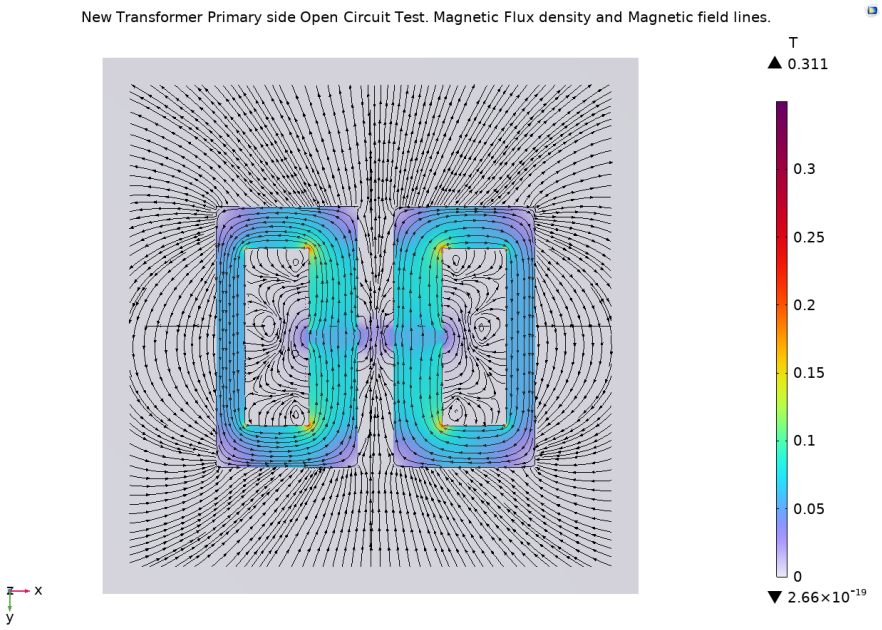

Figure 3.6 Magnetic flux density: primary-side open-circuit test, New Transformer.

In the figure, the core gap and resulting magnetic fringing are clearly visible. The three distinct primary windings can be identified by the three circular field patterns. The central winding appears distorted due to a simulation issue that failed to account for the inner five turns. While the peak flux density is higher than calculated, in general it in range of the predicted amount.

3.4 Construction

With the design finalized, the manufacturing and procurement of components could begin. The magnetic core and Litz wire were purchased, while the remaining components were custom-made in-house. The fabricated parts are shown in Figure 3.7.

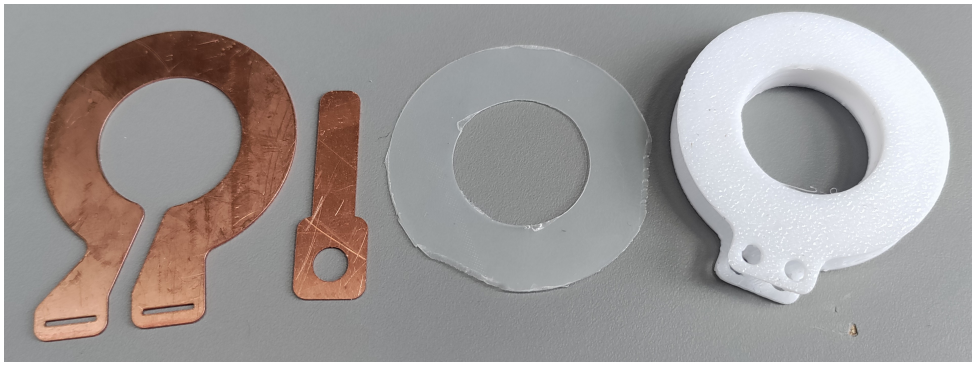

Figure 3.7 Custom-manufactured components. From left to right: Secondary winding, secondary connector, Mylar insulator, and plastic bobbin.

The secondary windings were manufactured using a laser cutter on copper sheet material. The Mylar insulator was cut using a precision cutter, and the plastic bobbin was 3D-printed in PLA as two separate halves, which were later glued together. Once all components were ready, they were assembled into the complete transformer, shown in Figure 3.8.

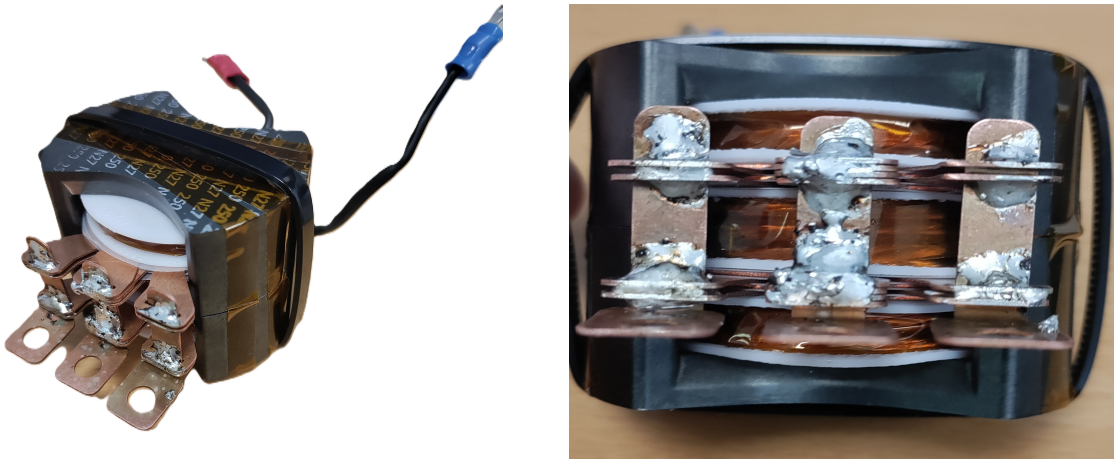

(a) New Transformer fully assembled. **(b)** Front secondary side

Figure 3.8 Fully assembled transformer.

As seen in Figure 3.8, the final build transformer has a footprint of approximately 50mm in width, 40mm in height, and 65mm in depth. This meets the design constraints outlined earlier. However, it should be noted that around 15mm of the total depth is contributed by the secondary connector, indicating a potential area for size optimization in future iterations.

4 Laboratory and Results

4.1 Testing and Results

With the new transformer fully assembled, it is now possible to begin real-world testing and compare the results to both simulation data and the performance of the PREMO transformer.

4.1.1 Impedance Analyzer Testing

To ensure consistency, the same tests performed on the PREMO transformer were repeated for the new transformer using an impedance analyzer. These tests focus exclusively on inductive parameters, as they are the only directly comparable outputs from the previous simulations. The new transformer placed in the impedance analyzer during the open-circuit test on the primary side is shown in Figure 4.1.

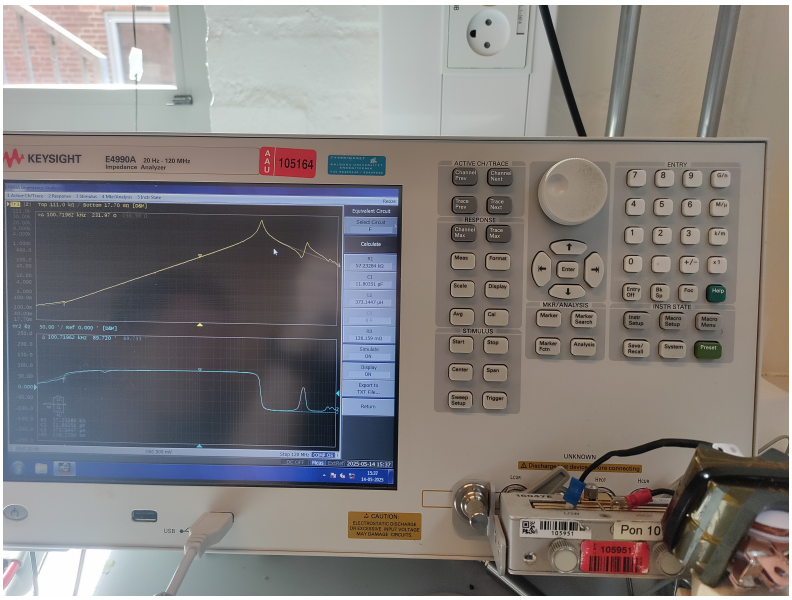

Figure 4.1 New transformer undergoing open-circuit test on the primary side using an impedance analyzer[8][9]

Results

The inductive parameters obtained from the impedance analyzer are presented in Table 4.1, alongside both calculated and simulated values, as well as comparable results from the PREMO transformer.

	Calculated	Simulated	Expriment	PREMO Exp	PREMO (Sim.)
$L_{pri,mag}$	0.4 mH	N/A	0.37 mH	0.9 mH	1.58 mH
$L_{pri,leak}$	N/A	N/A	16.3 µH	8.2 µH	16.2 uH
$L_{sec,mag}$	0.250 µH	0.298 µH	0.30 µH	1.31 µH	1.76 µH
$L_{sec,leak}$	N/A	194 nH	99 nH	135 nH	N/A

Table 4.1 Comparison of inductive parameters between the new Custom transformer and the PREMO transformers

The new transformer meets the design objectives by achieving a higher primary-side leakage inductance of 16.3 μH, compared to 8.2 μH in the PREMO transformer. Additionally, the secondary-side leakage inductance has been reduced from approximately 135 nH to 99 nH. The turns ratio has also been increased relative to the PREMO design, contributing to improved performance. Although simulation results varied significantly and did not allow for a definitive one-to-one comparison, the general trends align with the design goals. Further refinement of the simulation model is required to minimize discrepancies and improve accuracy.

4.2 Leakage Current Testing

Having determined the equivalent inductive parameters, the next step is to ensure electrical safety through leakage current testing. This test assesses the insulation quality by applying high voltage and monitoring the resulting current. The test setup is illustrated in Figure 4.2.

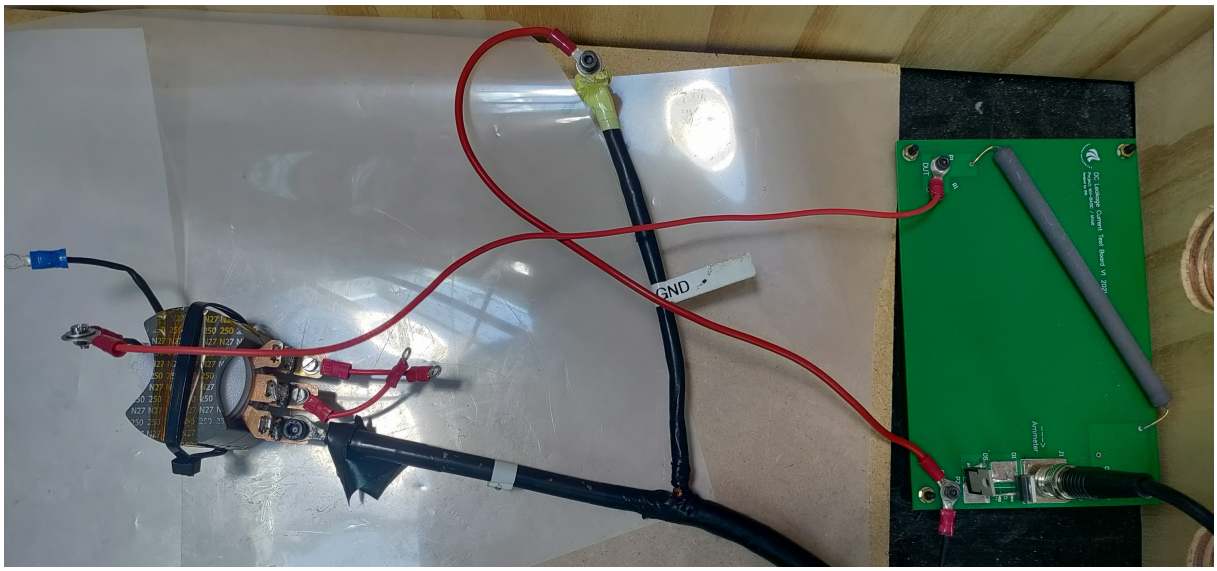

Figure 4.2 Leakage current test setup. The transformer is on the left, and the measurement board is on the right. A high-voltage power supply is connected via the black cable below.

The test goal is to achieve a voltage of 3 kV, and according to IEC 61558-1, the leakage current must not exceed 0.5 mA [21]. The results are shown in Figure 4.3.

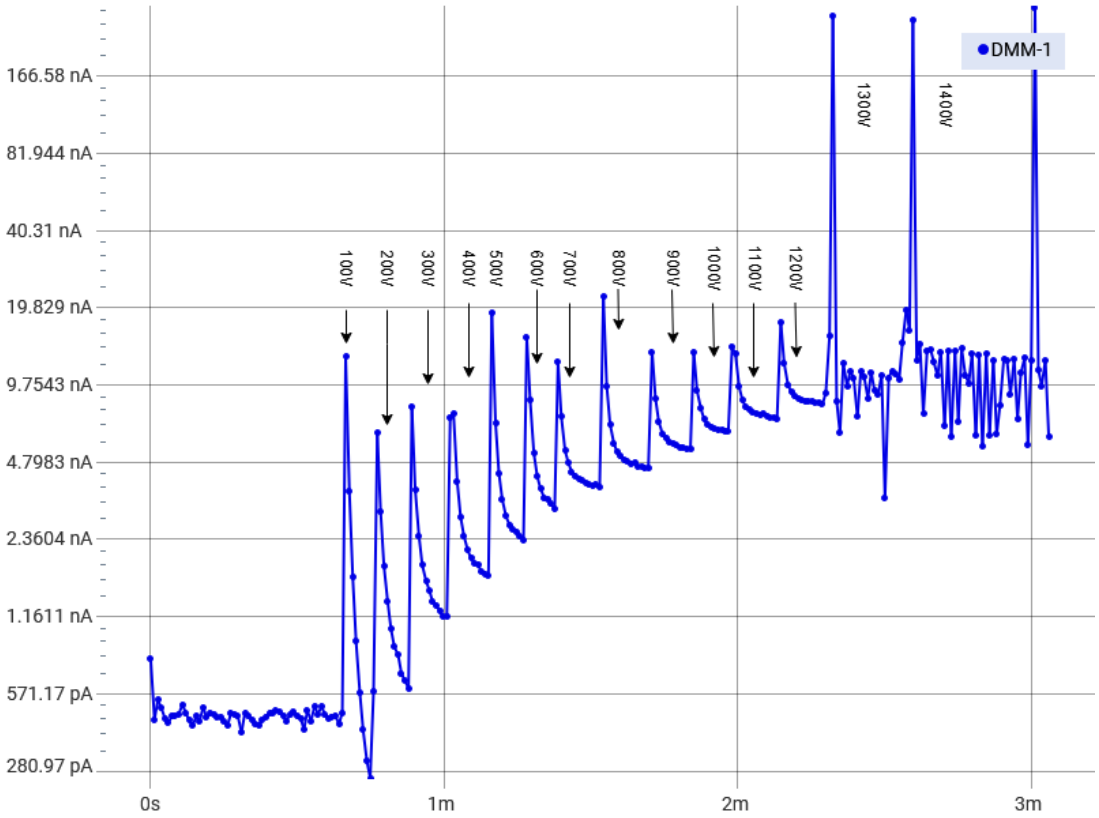

Figure 4.3 Leakage current test results from 0–1400 V in 100 V increments, for the New Transformer. Current is on the Y-axis and time on the X-axis.

The figure shows that each voltage step results in a transient current spike due to system capacitance charging. The insulation successfully withstood up to 1300 V, but partial discharge occurred at 1400 V. While this meets the requirements for testing in the converter, further insulation improvements are needed for a final product.

4.3 Turn Ratio Verification

To verify the transformer's turn ratio, it was connected to a function generator supplying an AC signal at 100 kHz. The voltage waveforms were measured on both the primary and secondary sides, as shown in Figure 4.4.

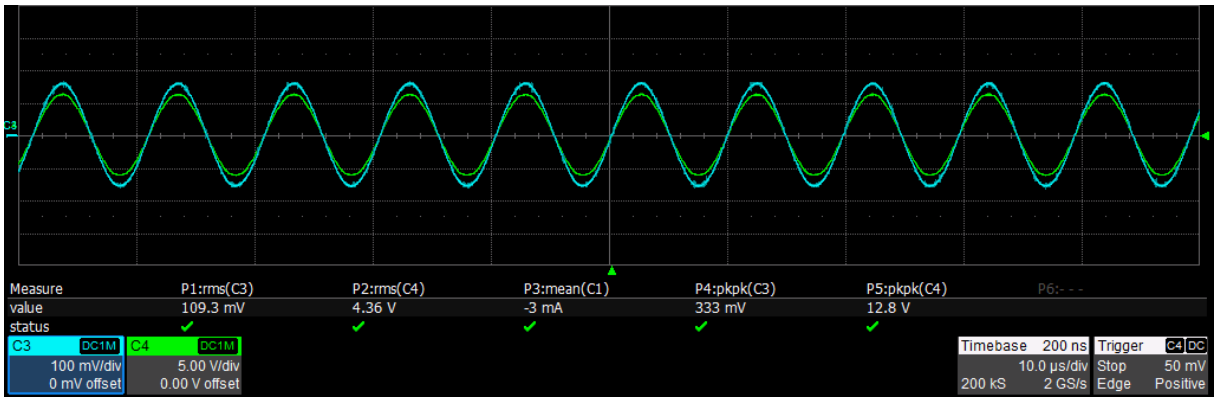

Figure 4.4 Turn ratio test. Channel C3 represents the secondary side, and C4 represents the primary side.

From the figure, the RMS voltage on the secondary side (C3) is 109.3 mV, while the primary side (C4) measures 4.36 V. The turn ratio is calculated as:

$$n = \frac{V_{\text{pri}}}{V_{\text{sec}}} = \frac{4360 \text{ mV}}{109.3 \text{ mV}} \approx 39.89 \tag{4.1}$$

The calculated turn ratio of 39.89 is considered acceptable, aligning closely with the design target of 40:1.

5 Discussion

In this chapter, the various methods, design decisions, and resulting outcomes are discussed in detail.

5.1 Simulation Accuracy and Challenges

Simulation results showed notable discrepancies when compared to experimental measurements, particularly for the PREMO transformer. The simulations consistently overestimated inductance values, likely due to incorrect core material parameters and simplifications in the model, such as idealized geometry and exaggerated spacing. These inaccuracies raise concerns about the reliability of simulation tools for precision transformer design. However, in the case of a fully planar transformer, simulation accuracy is expected to improve, as many of the variables associated with wire winding, such as inconsistent spacing and winding distribution—are eliminated.

5.2 Design Philosophy and Choices

The design process for the new transformer, outside the simulation environment, progressed smoothly. The physical prototype met its goals, achieving increased primary-side leakage inductance and reduced secondary-side leakage inductance. The decision to adopt a semi-planar structure proved effective. As previously noted, a fully planar transformer could offer higher simulation accuracy, but the complexity of stacking layers and ensuring consistent insulation presents practical challenges. Additionally, the use of a gapped core, while effective in controlling inductance, introduces increased magnetic reluctance and associated losses. Further investigation is warranted to determine if an ungapped core could deliver similar performance with reduced losses.

5.3 Design Process

The integration of simulation into the design process introduced new opportunities for digital iteration and a deeper understanding of design trade-offs. However, as the results demonstrate, if the simulation is not properly calibrated or based on accurate parameters, the effort and resources invested may not yield useful outcomes. Therefore, while simulations can enhance the development process, their application must be done with care and a clear understanding of their limitations.

5.4 Testing and Result Validation

Testing was conducted using an impedance analyzer, a standard tool for transformer characterization, which provided highly accurate and reliable results. The turn ratio was verified using a signal generator at high frequency, a straightforward method that is effective under no-

load conditions but requires further validation under operational load. The insulation integrity was assessed using a current leakage or voltage breakdown test, which offers a non-destructive and safe method of evaluation. The accuracy of this setup is largely attributed to the precision of the current sensor employed.

5.5 Comparison with Existing Solutions

The new transformer demonstrated promising performance during testing, especially when compared to the design used in the APG converter. The increased turns ratio and improved leakage characteristics represent potential advantages. However, real-world testing within the converter environment is essential to confirm these improvements. Significant work remains to validate the design under operational conditions and fully prove its effectiveness.

6 Conclusion

This project set out to develop a new transformer for a converter used in a remotely operated vehicle (ROV), addressing a key limitation in the original system, which was unable to meet the required voltage specifications. To overcome this challenge, a custom transformer was designed using modern digital engineering tools, including SolidWorks for CAD modeling and COMSOL Multiphysics for finite element simulations.

The development process began with a comprehensive analysis of the existing PREMO transformer [3], both experimentally using a Keysight impedance analyzer and virtually through COMSOL simulations. Although the simulation results differed significantly from the measured values—primarily due to uncertainties in the core material properties and modeling simplifications—they provided valuable insights into the design constraints and informed the conceptual direction of the new design.

A semi-planar transformer with a 40:1 turn ratio was successfully developed to replace the original unit. The new design focused on increasing the primary-side leakage inductance, reducing the secondary-side leakage inductance, and achieving a higher turn ratio, all while maintaining compatibility with the original form factor. Experimental testing validated that the new transformer achieved a 35% reduction in secondary leakage inductance, doubled the primary leakage inductance, and attained a measured turn ratio of 39.89. However, full implementation testing within the converter system could not be completed due to time constraints, leaving final system-level performance unverified.

Although one of the goals was to integrate simulation tools into the development workflow, the results varied considerably. This highlights the importance of accurate modeling, particularly for semi-planar designs, where CAD representations of wire windings may not fully capture physical realities. In contrast, fully planar designs may allow for more accurate simulation due to their geometric simplicity—this remains an area for future investigation.

In conclusion, the project successfully delivered a custom-designed transformer optimized for the specific requirements of a compact ROV power system. Despite limitations in simulation accuracy, the work represents a meaningful step forward in digitally guided transformer design and lays a foundation for future refinement and implementation.

7 Further work

Based on the findings and results presented in this report, the following steps are recommended to complete the development of the transformer for the APG converter:

Heating Simulation and Cooling Solution

Since the transformer operates within a sealed tube with no active airflow, thermal management becomes critical. A thermal simulation should be conducted preferably using COMSOL Multiphysics to evaluate heat generation under full load conditions and to design an appropriate passive or active cooling solution.

Refinement of Simulation Models

To improve accuracy in future designs, the simulation workflow in COMSOL should be further refined. This includes a better understanding of how to accurately simulate magnetic components and implement realistic boundary conditions. While not strictly necessary for the current design, this refinement could significantly reduce future design time and increase confidence in simulation-driven development.

Investigation of Core Materials and Gapping

Further investigation into alternative core materials and gapping strategies is needed. Specifically, testing an ungapped version of the core could help assess how the presence or absence of an air gap impacts core losses, inductance, and overall transformer performance.

Integration with Converter System

The next step is to integrate the transformer into the actual APG converter system. This test will verify whether the transformer can support output voltages up to 1000 V and deliver power levels up to 2 kW. It will also help evaluate overall converter performance improvements resulting from the new transformer design.

Redesign for Higher Voltage Protection

The measured breakdown voltage was approximately 1400 V, which may be insufficient for certain high-voltage applications. A redesign of the insulation or winding separation strategy is recommended to increase the breakdown voltage margin and ensure safe operation under all expected conditions.

Bibliography

[1] "Remote operated vehicle market strategic analysis and growth opportunities," 2025. [Online]. Available: https://www.towardsautomotive.com/insights/remote-operated-vehicle-market-sizing

[2] AAL Power Group, "Aal power group," 2025, accessed: 2025-05-21. [Online]. Available: https://www.aalpowergroup.com/

[3] Premo, "Dcdc214-002 datasheet," 2023, accessed: 2025-05-21. [Online]. Available: https://media.digikey.com/pdf/Data%20Sheets/Premo%20PDFs/DCDC214-002.pdf

[4] "Phase-shifted full bridge dc/dc power converter design guide," 2014. [Online]. Available: https://www.ti.com/lit/ug/tidu248/tidu248.pdf

[5] T. Brander, A. Gerfer, B. Rall, and H. Zenkner, *Trilogy of magnetics*. Würth Elektrinik eiSos Gmbh & Co. KG, 2018, vol. 5th edition.

[6] W. Hurley and W. W?lfle, *Transformers and Inductors for Power Electronics: Theory, Design and Applications*, 1st ed. New York: Wiley, 2013.

[7] Elektrisola Dr. Gerd Schildbach GmbH & Co KG, "Litz wire, hf-litz, high frequency litz wire, litz wire for high efficiency," 2025, accessed: 2025-05-21. [Online]. Available: https://www.elektrisola.com/en/Litz-Wire/Info

[8] Keysight Technologies, *Keysight E4990A Impedance Analyzer*, 2023, accessed: 2025-05-21. [Online]. Available: https://www.keysight.com/us/en/product/E4990A/impedance-analyzer-20-hz-to-120-mhz.html

[9] ——, *Keysight 16047E Test Fixture*, 2023, accessed: 2025-05-21. [Online]. Available: https://www.keysight.com/us/en/product/16047E/test-fixture-for-impedance-measurements.html

[10] COMSOL Inc., "Comsol multiphysics," 2025, accessed: 2025-05-21. [Online]. Available: https://www.comsol.com/

[11] Dassault Systèmes, "Solidworks," 2023, accessed: 2025-05-21. [Online]. Available: https://www.solidworks.com/

[12] "Pm 50/39 core and accessories," 2013. [Online]. Available: https://docs.rs-online.com/46da/0900766b813c0ccf.pdf

[13] D. Serrano, H. Li, S. Wang, T. Guillod, M. Luo, V. Bansal, N. K. Jha, Y. Chen, C. R. Sullivan, and M. Chen, "Why magnet: Quantifying the complexity of modeling power magnetic material characteristics," *IEEE Transactions on Power Electronics*, vol. 38, no. 11, pp. 14 292–14 316, 2023.

[14] H. Li, D. Serrano, T. Guillod, S. Wang, E. Dogariu, A. Nadler, M. Luo, V. Bansal, N. K. Jha, Y. Chen, C. R. Sullivan, and M. Chen, "How magnet: Machine learning framework for modeling power magnetic material characteristics," *IEEE Transactions on Power Electronics*, vol. 38, no. 12, pp. 15 829–15 853, 2023.

[15] H. Li, D. Serrano, S. Wang, and M. Chen, "Magnet-ai: Neural network as datasheet for magnetics modeling and material recommendation," *IEEE Transactions on Power Electronics*, vol. 38, no. 12, pp. 15 854–15 869, 2023.

[16] "Cli 200/120," 2025. [Online]. Available: https://www.block.eu/en_EN/productversion/cli-200120

[17] C. W. T. McLyman, *Transformer and Inductor Design Handbook, Fourth Edition.*, fourth edition. ed. Boca Raton, FL: CRC Press, 2017.

[18] "Mylar® 100a – 0.1mm — dupont™," 2017. [Online]. Available: https://materials-direct.com/wp-content/uploads/2019/08/MylarA_Datsheet.pdf

[19] "Technical data by size," 2025. [Online]. Available: https://www.elektrisola.com/en/Products/Enamelled-Wire/Technical-Data#iec60317

[20] "Kapton summary of properties," 2025. [Online]. Available: https://www.dupont.com/content/dam/electronics/amer/us/en/electronics/public/documents/en/EI-10142_Kapton-Summary-of-Properties.pdf

[21] *Safety of transformers, reactors, power supply units and combinations thereof – Part 1: General requirements and tests*, International Electrotechnical Commission Std. 61 558-1, 2017.

A COMSOL Simulation

To perform the simulation, a well-designed 3D CAD model must first be created. Once the model is ready, open COMSOL and start a new blank model.

Step 1: Importing the CAD Model

The first step is to import the CAD model into COMSOL. If the model contains too many components or unnecessary details, the *Delete* function can be used to simplify the geometry.

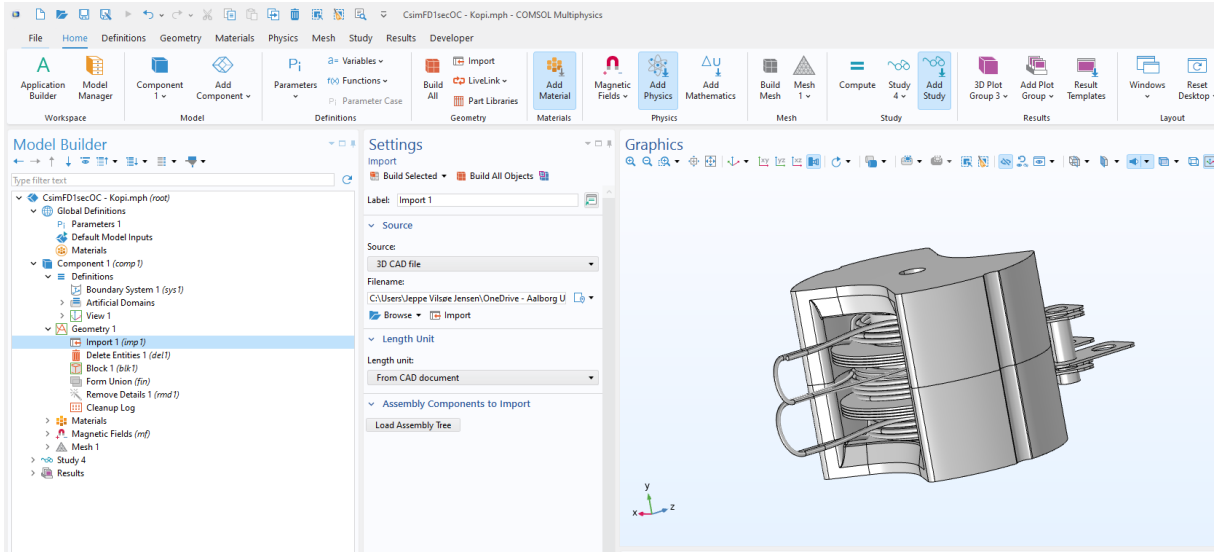

Figure A.0.1 Importing the model into COMSOL

Step 2: Creating the Simulation Domain

Create a block that represents the air volume surrounding the transformer. Use the *Layers* function to add space on all sides of the geometry. Then, under the *Definitions* section, add an **Infinite Element Domain**. This ensures that the magnetic field lines are not artificially constrained by the physical boundaries of the block.

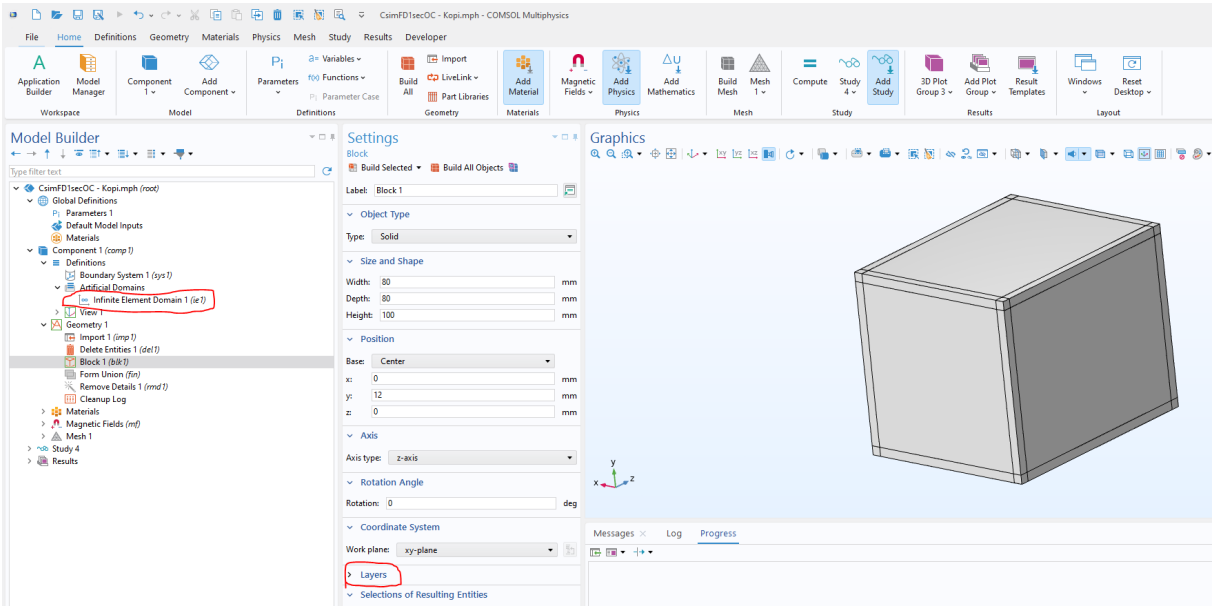

Figure A.0.2 Defining the simulation domain and applying the infinite element domain

Step 3: Assigning Materials

Assign the appropriate materials to each part of the geometry. In this case:

- **Air** is assigned to the surrounding domain.
- **Core material** is assigned to the magnetic core.
- **Copper** is used for the windings.

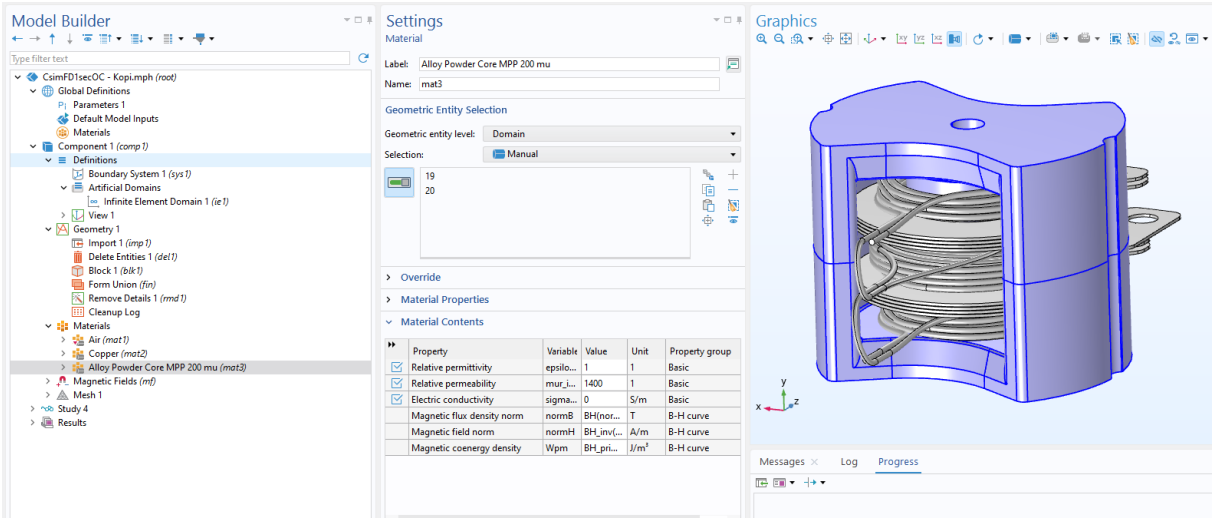

Figure A.0.3 Material assignment in the model

Step 4: Adding Physics

The next step is to define the physics of the model. Select **Magnetic Fields (mf)** as the physics interface.

- Add **Ampère's Law** and apply it to all relevant domains.
- Define the coils in the system, specifying them as *Single-Turn* or *Multi-Turn* coils as

needed.

- Set the input parameters for each coil, such as current or voltage excitation.

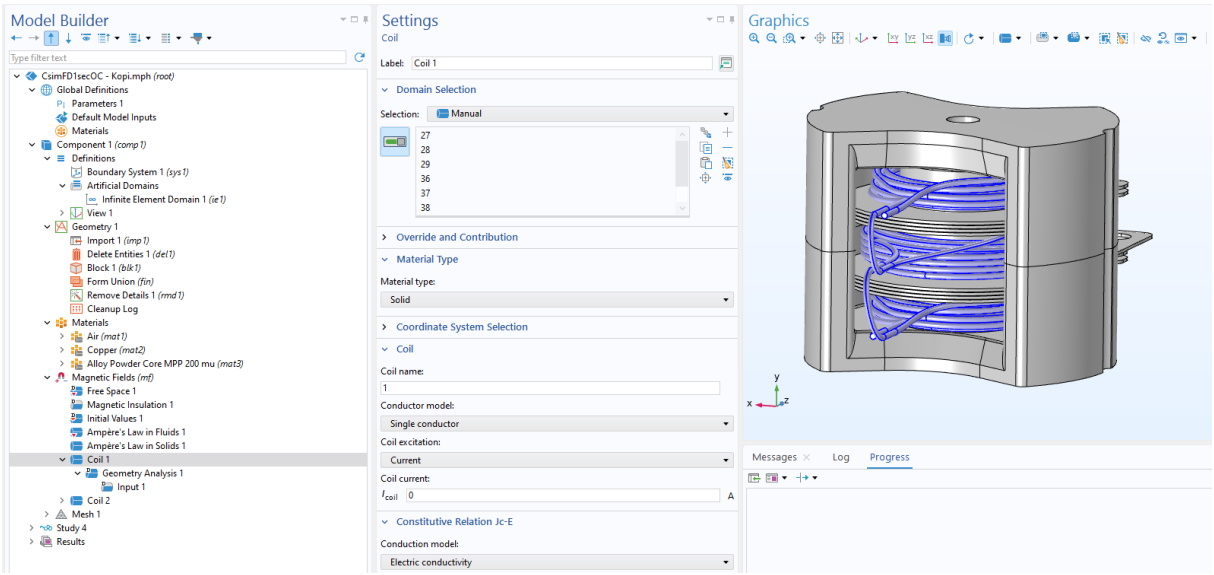

Figure A.0.4 Setting up magnetic physics and coil inputs

Step 5: Meshing and Running the Simulation

Generate the mesh that will be used for the numerical solution. The mesh determines the resolution of the solution space:

- A finer mesh yields more accurate results but increases simulation time.
- In this case, the **Coarse** mesh setting was selected, leading to a simulation time of approximately 1.5 hours.

After meshing, add the necessary simulation *studies*:

1. **Coil Geometry Analysis** – required when modeling coil domains.
2. **Small-Signal Analysis, Frequency Domain** – used to evaluate the frequency response and impedance characteristics.

In the second study, define the input frequency range of interest. Once the setup is complete, the simulation can be run.

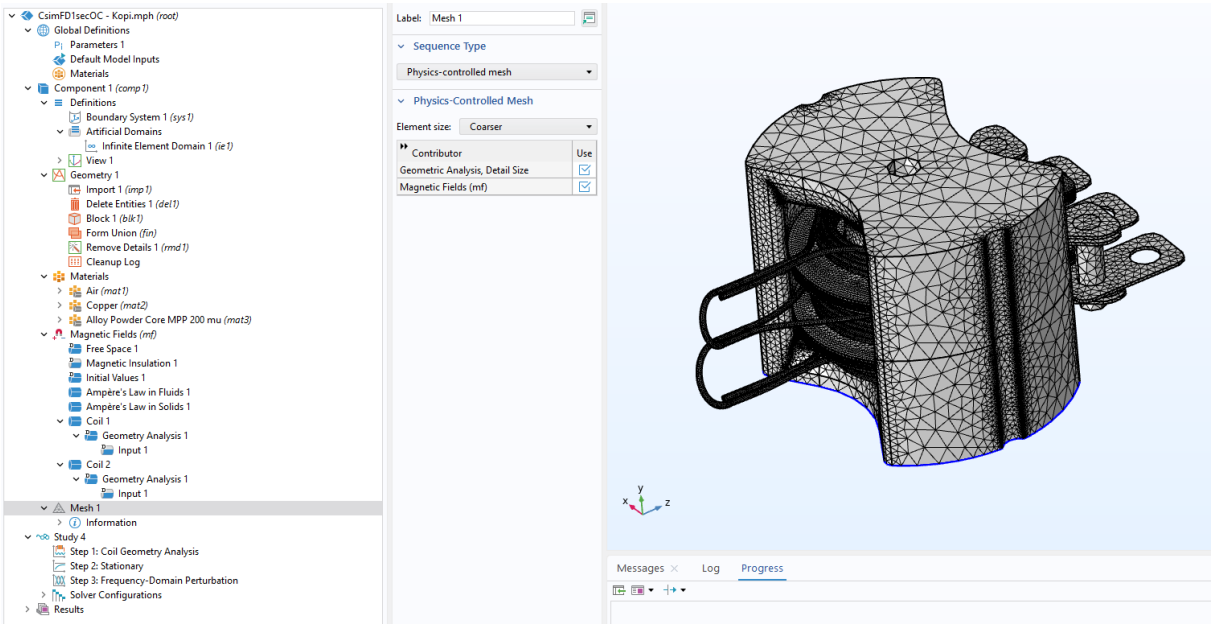

Figure A.0.5 Meshing and adding the simulation studies